Mol Divers (2013) 17:515–524
DOI 10.1007/s11030-013-9452-z

FULL-LENGTH PAPER

Salvianolic acid A, a polyphenolic derivative from *Salvia miltiorrhiza* bunge, as a multifunctional agent for the treatment of Alzheimer's disease

Ying Ying Cao · Ling Wang · Hu Ge · Xi Lin Lu · Zhong Pei · Qiong Gu · Jun Xu

Received: 26 April 2013 / Accepted: 6 May 2013 / Published online: 24 May 2013

Abstract The effects of Salvianolic acid A (Sal A) on the treatment of Alzheimer's disease (AD) were investigated. Sal A significantly inhibits amyloid beta (Aβ) self-aggregation and disaggregates pre-formed Aβ fibrils, reduces metal-induced Aβ aggregation through chelating metal ions, and blocks the formation of reactive oxygen species (ROS) in SH-SY5Y cells. Sal A protects cells against Aβ_{42}-induced toxicity. Furthermore, Sal A, possibly because of the effects of decreasing toxicity effects of Aβ species, alleviates Aβ-induced paralysis in transgenic *Caenorhabditis elegans*. Circular dichroism (CD) experiments and Molecular dynamic (MD) simulations demonstrate that Sal A inhibits Aβ self-aggregation through binding to the C-terminus of Aβ, and therefore stabilizing the α-helical conformations. Altogether, our data show that Sal A, as the multifunctional agent, is likely to be promising therapeutics for AD.

Keywords Alzheimer's disease · Salvianolic acid A · Amyloid β · Anti-oxidant · Neuroprotecitve

Introduction

Alzheimer's disease (AD) is a progressive neurodegenerative disorder characterized by extracellular amyloid beta (Aβ) plaques, intracellular neurofibrillary tangles, and soluble Aβ oligomers [1,2]. Abnormal production and aggregation of Aβ are essential pathogenic events in AD [3–5]. Moreover, Aβ can induce oxidative stress and inflammation in the brain [6,7].

In addition to Aβ aggregation, the abnormal concentrations of metal ions, such as iron, copper, and zinc ions, occur in significant amounts in AD brains [8]. High metal ion concentrations play important roles in Aβ aggregation, deposition, and neurotoxicity, and induce ROS [9–12]. A number of in vivo studies have shown that copper, iron, and zinc ions can cause oxidative damage to neuronal cells [13,14]. Modulation of metal ions in the brain can be an effective therapeutic strategy for AD. Metal chelating agents have the potential ability to regulate, both in vitro and in vivo, metal ion-induced Aβ aggregation and neurotoxicity [15]. Metal ion chelators, such as clioquinol (CQ) and 8-hydroxyquinoline derivatives [16], have been moved into clinical trials [17]. However, long-term use of CQ brings adverse side effects [18].

Oxidative stress also plays an important role in the pathogenesis of AD [19–21]. The brain is highly sensitive to oxidative stress. The brain of an AD patient loses synapses, and is particularly vulnerable to oxidative damage [22–24]. Oxidative stress promotes Aβ toxicity through the production of free radicals. The inhibitory effects of Aβ depositions by anti-oxidants have been demonstrated through both in vitro assays and transgenic mouse models [25]. As free radical scavengers, polyphenols have therapeutic effects with regard to chronic and degenerative diseases [26]. Moreover, the anti-amyloid aggregation effects of polyphenols are significantly related to their anti-oxidative capabilities [27].

Salvianolic acid A (Sal A) is one of the main biochemically active ingredients isolated from the root of *Salvia miltiorrhiza* Bunge (also known as Danshen) [28]. It has been reported that Sal A is anti-oxidative [29], anti-apoptotic [30], and anti-inflammatory [31]. Moreover, Sal A inhibits Src-family SH2 domain mediated protein-protein interactions [32], and protects human SH-SY5Y neuroblastoma

Y. Y. Cao · L. Wang · H. Ge · Q. Gu (✉) · J. Xu
Research Center for Drug Discovery, School of Pharmaceutical Sciences, Sun Yat-Sen University, Guangzhou 510006, China
e-mail: guqiong@mail.sysu.edu.cn

X. L. Lu · Z. Pei
Neurology Department of the First Affiliated Hospital, Sun Yat-Sen University, Guangzhou 510080, China

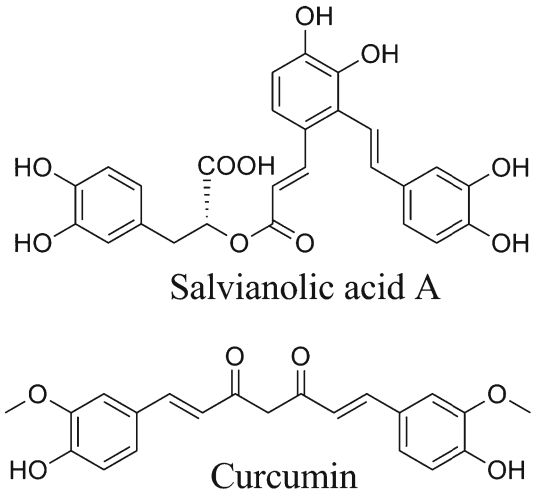

Fig. 1 Structures of salvianolic acid A and curcumin

cells against H_2O_2-induced injury by increasing stress tolerance ability [33].

Sal A and curcumin are structurally similar; both contain caffeic acid as a common scaffold (Fig. 1). It is known that curcumin is an anti-Aβ aggregation agent [34]. Consequently, we hypothesized that Sal A can also inhibit the Aβ aggregation. To test our hypothesis, we conducted a number of experiments to evaluate Sal A's anti-Aβ aggregation mechanisms of action (if any). Our results show that Sal A significantly inhibits Aβ aggregation, protect Aβ-induced neurotoxicity, and ameliorate Aβ-induced paralysis in a *C. elegans* model. Molecular dynamics (MD) simulations demonstrate that Sal A stabilizes the α-helical conformations of Aβ by binding to its C-terminus. Further experiments reveal that Sal A is a multifunctional agent for the treatment of Alzheimer's disease.

Methods

General experimental procedures

Aβ_{42} was purchased from Annaspec, Inc. (Fremont, CA). Sal A (purity > 98 %) was purchased from Chengdu Mansite Biotech Co. Ltd., dissolved in DMSO to 10 mM, and stored at −20 °C. Thioflavin T, DCFH-DA, t-BuOOH, dimethyl sulfoxide (DMSO), and MTT were purchased from Sigma (St. Louis, MO, USA). CL4176 (genetically modified *C. elegans*) was obtained from The Caenorhabditis Genetics Center (CGC) (Minneapolis, MN). Other reagents were commercially available, and were analytical grade without further processing.

Peptide preparation

For the Thioflavin T (ThT), circular dichroism (CD), transmission electron microscopy (TEM), and metal-induced Aβ_{42} aggregation experiments, Aβ_{42} powder was initially dissolved to 440 μM in 1 %NH_3-H_2O and stored at −80°C. The peptide solution was diluted to certain concentrations with 20 mM PBS (pH = 7.4). For the MTT SH-SY5Y cell metabolic activity experiments, Aβ_{42} powder was initially dissolved to 2 mM in DMSO, and then diluted to certain concentrations with DMEM. To get Aβ_{42} fibrils, Aβ_{42} was incubated in 20 mM PBS, at 37°C, for 48 h.

ThT fluorescence assay

ThT-induced fluorescence changes were measured to quantify amyloid fibril formation using a multifunctional microplate reader Therme type (the Ruishi Di Ken). To determine amyloid aggregation and fibril formation, the solutions containing Aβ_{42}, with or without Sal A or curcumin, were added to 5 μM ThT in 50 mM glycine–NaOH solution (pH = 8.5), in a final concentration volume of 200 μL. Each assay was run in triplicate and fluorescence intensities were measured at excitation and emission wavelengths of 450 and 485 nm.

CD spectroscopy

Modification in the secondary structure of Aβ_{42}, with or without Sal A, was recorded for 48 h using a Jasco-810-150S spectropolarimeter (JASCO, Tokyo Japan). Sal A was dissolved and diluted with methanol. 150 μL Aβ_{42} (100 μM) in phosphate buffer containing NaH_2PO_4, Na_2HPO_4, and methanol was prepared to monitor the structure of Aβ_{42} in the absence or presence of an equal amount of 200 μM Sal A, at 37 °C for 0 h and 48 h (creating a total of four samples). Each sample was diluted to 750 μL with pH 7.4 phosphate buffer; this buffer was also the blank control. CD spectrum was scanned using a 750 μL quartz cuvette; path length was 10 mm and the wavelength range was set at 190–260 nm. Average spectra were smoothed with the means-movement algorithm in the Jasco spectrum analysis program.

TEM imaging

TEM was used to detect the disaggregation effect of Sal A on Aβ_{42} pre-formed fibrils. 10 μL and 100 μM aggregated Aβ_{42} was mixed with or without equal amounts of 100 or 50 μM Sal A, and incubated at 37 °C for 24 h. Following incubation, 5 μL of duplicate samples were applied to 300-mesh copper grids for 1 min; excess samples were wicked off, and the grids were washed with ultrapure water and negatively stained with 2 % uranyl acetate solution for 1 min. The staining solution was absorbed with filter paper. The grids were then observed using TEM (JEOL JEM-1400, USA) at 120 kV, with 100 or 200 nm scan bar.

Molecular dynamics (MD) stimulations

The initial structure of Aβ was taken from the NMR structure. The structure were assigned in the Amber force field with Kollman-united-atom charge strained in solution (PDB entry 1BA4) [34]. The atom types and potentials were encoded in Sybyl 7.3 [35]. The initial structures of Sal A were optimized using an MMFF force field [36], and the Powell method was used for energy minimization via default parameters in Discovery Studio. 2.5 [37]. Autodock 4.0 [38] was employed to identify the binding poses of Sal A for Aβ_{42} with a Lamarckian genetic algorithm. The grid map, with $80 \times 80 \times 80$ points spaced equally at 0.375 Å, was generated using the AutoGrid program to evaluate the binding energies between ligand and receptor. All docked poses of Sal A were clustered using a tolerance of 2 Å for root mean square deviation (RMSD), and were ranked based on binding docking energies. The lowest energy conformation in the most populated cluster was chosen for MD simulations, which were carried out using the GROMACS 4.5.3 package [39], with constant number, pressure, and temperature (NPT), and periodic boundary condition. The AMBER ff03 force field [40] was applied for peptides. Parameters for Sal A were obtained from the ANTECHAMBER module using the Generalized Amber force field (GAFF) [41]. The partial atomic charges for the ligand atoms were assigned using RESP charge-fitting procedure, with input from Hartree–Fock calculations at the 6-31G* level (through use of the Gaussian03 program [42]). During the simulations, the pressure and the temperature were coupled to 1 bar, with an anisotropic coupling time of 1.0 ps, and kept at 300 K with a coupling time of 0.1 ps. The coordinates of the whole 90 ns MD run were saved every 2 ps.

Metal-chelating properties assay

In the metal-chelating experiment, $CuSO_4$, $Fe_2(SO4)_3$, $ZnSO_4$, and Sal A were dissolved to 1 mM with ethanol. The absorption spectra of 10 μM Sal A, with or without 10 μM Cu (II), Fe (III), and Zn (II), were measured at room temperature using a UV–visible spectrophotometer UV-2450 (SHIMADZC Company, Japan) in a 1 cm quartz cell.

Metal-induced Aβ_{42} aggregation assay

In this assay, the solution of Zn^{2+}, Cu^{2+}, and Fe^{3+} was diluted with PBS at a pH value of 7.4. The final concentrations of Aβ_{42} and metal ions were 20 and 50 μM, respectively. Sal A was initially dissolved in DMSO to 10 mM with PBS. To study the effects of Sal A on metal-induced Aβ_{42} aggregation, Aβ_{42} was co-incubated with 50 μM Zn^{2+}, Cu^{2+} and Fe^{3+}, with and without Sal A, at 37 °C for 45 min. After the incubation, the fluorescence was measured with a multifunctional microplate absorption value in a 96-well plate (black plate) at excitation and emission wavelengths of 450 and 485 nm.

Anti-oxidation activity

Intracellular ROS was measured with the a fluorescent probe (2′,7′-dichlorofluorescein diacetate, DCFH-DA). Human neuroblastoma cells, SH-SY5Y, were grown at 37 °C in a humidified incubator with 5 % CO_2 in Dulbecco's modified Eagle's medium (DMEM, GIBCO), which contained 15 nonessential amino acid, and was supplemented with 10 % fetal calf serum (FCS, GIBCO), 1 mM glutamine, 50 mg/μL penicillin, and 50 mg/μL streptomycin. For assays, SH-SY5Y cells were cultured in 96-well plates at a seeding density of 1×10^5 cells per well. After 24 h, the cells were treated with Sal A and curcumin at various concentrations. The vehicle, as the control, was used in an extensive study of the markers of cell death after 24 h exposure. After 24 h of treatment with the compounds, the cells were washed with PBS and then incubated with 5 μM DCFH-DA in PBS at 37 °C in 5 % CO_2 for 30 min. After the DCFH-DA was removed, the cells were washed and incubated with 5 μM *t*-BuOOH in PBS for 30 min. At the end of incubation, the fluorescence of the cells from each well was measured at 488 nm excitation, and 525 nm emission, with a monochromator-based multimode microplate reader (INFINITE M1000). Results are expressed as a percentage of the sample average divided by the control group data, calculated as follows: (ODsample-ODblank) / (ODcontrol-ODblank) × 100 %.

Cell culture

SH-SY5Y neuroblastoma cells were used for the neurotoxicity assay. SH-SY5Y cells were plated in 96-well plates at a density of 5×10^4 cells/mL in Dulbecco's modified Eagle's medium (DMEM). Plates were incubated at 37 °C for 24 h to allow the cells to attach. After the original medium was removed, 100 μL of Sal A, with different concentrations, were added to individual wells. The same volume medium was added to the blank control wells. The cells and medium were added to the negative control wells. These plates were then incubated at 37 °C, in a 5 % CO_2 incubator, for another 48 h. Cell viability was determined using an MTT assay with an addition of 10 μL of 5 mg/mL MTT to each well, and further incubated for 4 h. The supernatant was discarded and 100 μL of DMSO were added to each well. The plates were oscillated so that the resultant formazan was fully dissolved. Absorbance value was measured at wavelength of 570 nm through a whole wavelength microplate reader, PowerWave XS2 (Bio-tech Company). Survival rate of cells was calculated via the following formula: cell survival rate(%) = (OD sample-OD blank)/(OD control-OD blank) × 100 %.

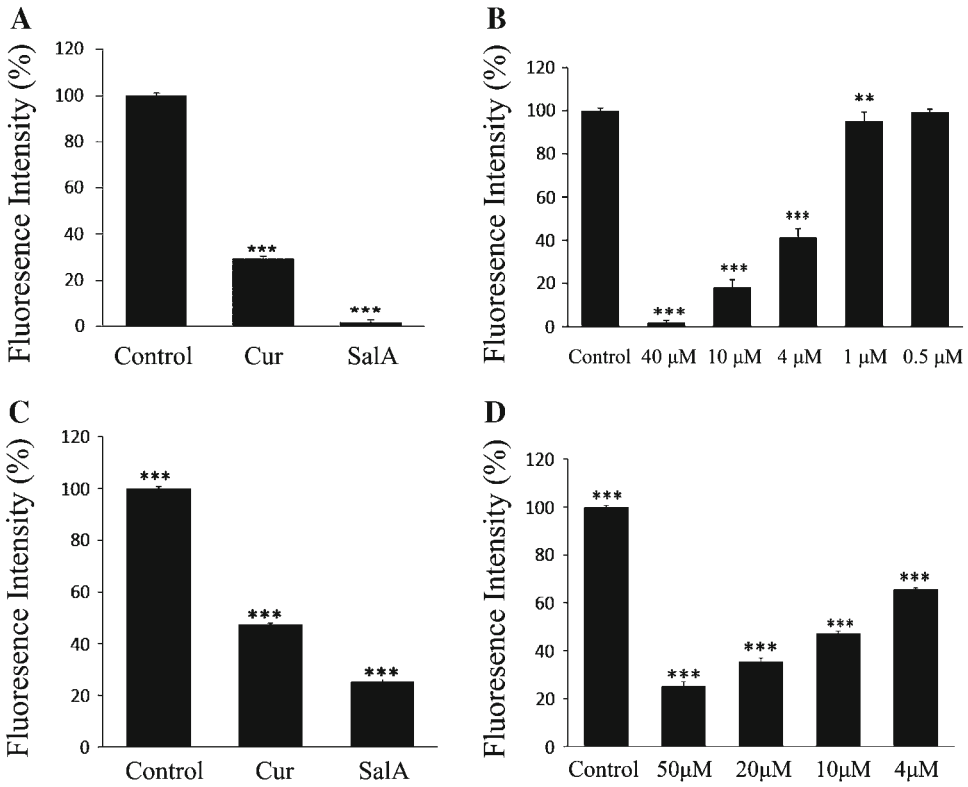

Fig. 2 Sal A inhibits Aβ_{42} aggregation and disaggregates pre-formed fibrils. ThT fluorescence assays were used to monitor the aggregated Aβ_{42} with excitation of 450 nm and emission of 485 nm. **a** The inhibition of Aβ_{42} aggregation compared with curcumin (Cur) (Cur at 50 μM, Sal A at 40 μM); **b** The Aβ_{42} aggregation inhibition at varied concentrations of Sal A; **c** The disaggregation of Aβ_{42} pre-formed fibrils compared with curcumin at 50 μM; **d** The disaggregation of Aβ_{42} pre-formed fibrils in dose-dependent manner. Data represent mean ± SEM from 5 independent experiments. $^{***}P < 0.001$ compared to samples without co-incubation with Sal A

Determination of neuroprotective activity

Aβ_{42} was dissolved to 2 mM with DMSO and further diluted into 100 μL of 40, 20 μM, and 10 μM, with Dulbecco's modified Eagle's medium, respectively. 0.8 μM DMSO were added to 100 μL Dulbecco's modified Eagle's medium to give the blank control. 100 μL Aβ_{42} of 40, 20, 10 μM, and the blank control were pre-incubated for 48 h for aging fibrils at 37 °C (as prepared in aggregation studies). Aggregated Aβ42 (40 20, 10 μM) were added to the SH-SY5Y cells, which had been incubated for 24 h. Absorbance value was measured at 570 nm through MTT methods. To study the protective effect of Sal A on the neurotoxicity of Aβ_{42}, 20 μM Aβ_{42} seed samples, with or without Sal A (10–80 μM), were pre-incubated at 37 °C for 48 h. Then the prepared samples were added to SH-SY5Y cells, and incubated at 37 °C for 48 h. DMSO diluted with PBS solution was also added to the blank control wells. The final concentration of DMSO in each well was less than 0.5 %. At the end of the experiment, samples were tested via MTT methods. Absorbance value was measured to determine cell viability.

Caenorhabditis elegans paralysis assay

The transgenic nematode strain, CL4176, was used for our paralysis assay. CL4176 was propagated at 15 °C on solid nematode growth medium (NGM), which was seeded with 200 μL OP50 (*Escherichia coli* strain) as food for each plate. To prepare age-synchronized worms, nematodes were transferred to fresh NGM plates on reaching reproductive maturity at 3 days of age, and allowed to lay eggs for 4–6 h. The CL4176 maintained at 15 °C was egg-synchronized onto the 35 × 10 mm culture plates, containing either a vehicle or Sal A. Transgenic expression was induced by upshifting the temperature from 15 to 26 °C for another 36 h after egg laying; this upshifting lasted until the end of the paralysis assay. Sal A was initially dissolved with DMSO, and then diluted 1,000 fold (with OP50 broth) to the final concentration (400 μL OP50 broth was added to 0.4 μL mother liquor, and the blank control group was 0.4 μL DMSO added to 400 μL OP50 broth). The final concentration of DMSO in the food did not exceed 0.1 %. The above mixture was added to NGM dish seed, with 200 μL OP50 for food in each plate. The NGM dish was placed on the table to dry. After 24 h of synchronization, the CL4176 were washed down with 1 mL ddH_2O, and transferred to the NGM dish seed, with or without 200 μL varied concentrations of Sal A. About 25 nematodes in each dish were cultured at 15 °C. After hatching for 36 h (12 h after administration), the NGM dishes were transferred to a 26 °C incubator. After another 36 h of changing temperature, paralysis was scored at 2 h intervals until the blank control group nematodes were all nearly paralyzed.

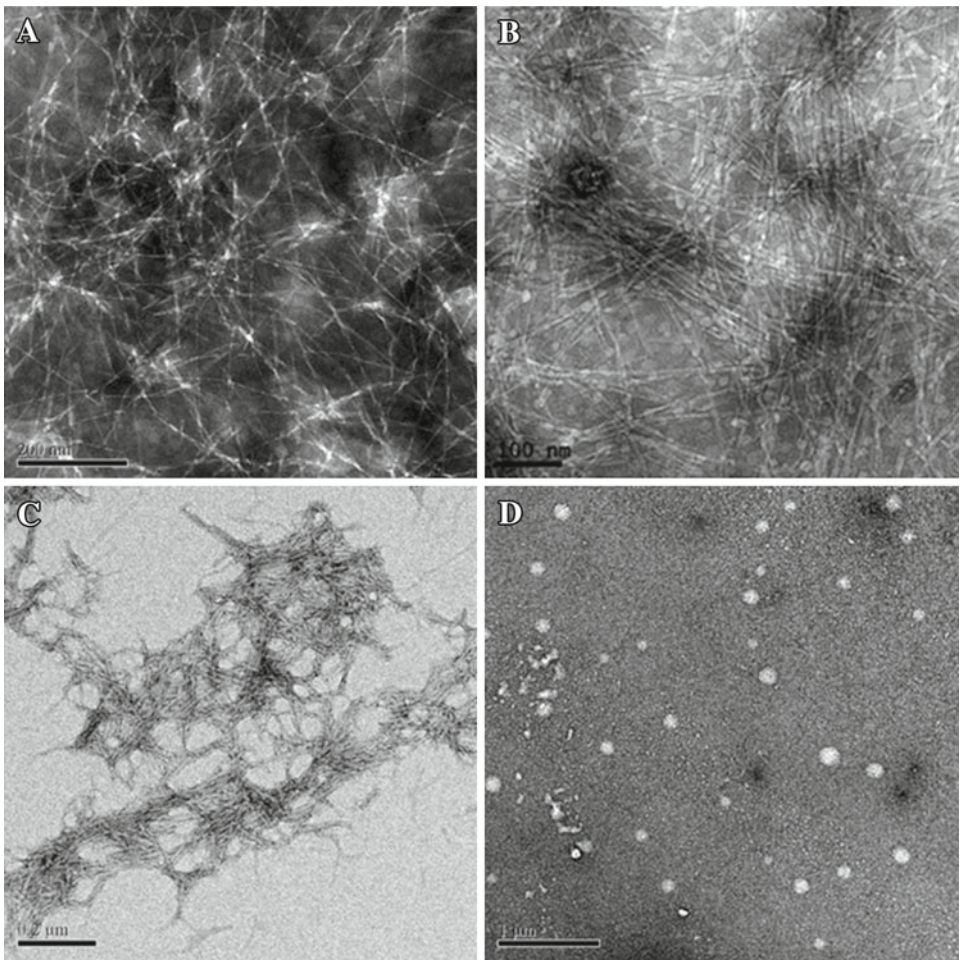

Fig. 3 Sal A disaggregates Aβ_{42} aging fibrils. The experiments were conducted for 100 μM Aβ_{42} at 37 °C. **a** Aβ_{42} fibrils incubated for 48 h without Sal A treatment; **b** Aβ_{42} fibrils incubated for 72 h without Sal A treatment; **c** Aβ_{42} fibrils incubated for 48 h, then further incubated for 24 h with 50 μM Sal A; **d** Aβ_{42} fibrils incubated for 48 h, then further incubated for 24 h with 100 μM Sal A

Western blotting

The total Aß in the transgenic *C. elegans* strains were identified through immunoblotting, using a Tricine-SDS-PAGE gel and the standard Western blotting protocol. After the experimental treatments, the worms were washed with distilled water, quickly frozen in liquid nitrogen, and sonicated in cell lysis buffer (50 mM HEPES, pH 7.5, 6 mM MgCl2, 1 mM EDTA, 75 Mm benzamide, 1mM benzamide, 1 mM DTT, 1 % Triton X-100) with protease inhibitor cocktail (sigma, Saint Louis, MO). The samples were then heated with loading buffer containing 5 % ß-mercaptoethanol (2:1; Bio-Rad, Hercules, CA). After mixing with the loading buffer, proteins were loaded in each lane. The membranes were probed with a primary anti-Aß antibody 6E10 (1:1000), followed by corresponding secondary antibodies.

Statistical analysis

The results were expressed as means ± SD, calculated from the specified numbers of determination. Statistically significant differences between experimental and control groups were detected through the Student's t test; p-values of less than 0.05 ($p < 0.05$) are considered significant.

Results

Sal A inhibits Aβ_{42} self-mediated aggregation and disaggregated Aβ_{42} aging fibrils

To determine whether Sal A reduces Aβ_{42} aggregation, the ThT fluorescence assay was conducted to examine Aβ_{42} fibril formation (Fig. 2a). The results demonstrate that Sal A is more potent (98 % at 40 μM) than curcumin (70 % at 50 μM) in inhibiting Aβ aggregation. Moreover, Sal A inhibits Aβ aggregation in a dose-dependent manner, with an IC_{50} value of $1-4$ μM (Fig. 2b). Sal A also dose dependently disaggregates fibrils aging. In this context, at concentrations of 50 μM, Sal A is also more potent than curcumin (Figs. 2c, d).

TEM was employed to probe Aβ_{42} disaggregation, by means of detecting Aβ_{42} morphologies, in the presence or absence of Sal A. Figure 3a and b demonstrate Aβ_{42} fib-

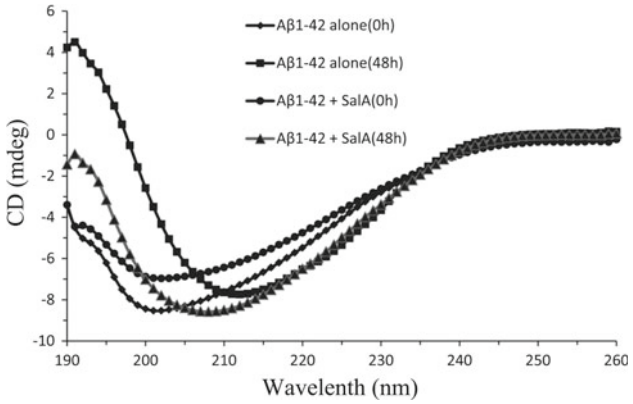

Fig. 4 CD spectra of Aβ_{42} with or without Sal A. CD spectra at 0 and 48 h were recorded with the wavelength range of 190–260 nm. The concentration Aβ_{42} in PBS was 20 μM. The concentration of Sal A added to the PBS was 40 μM

rils generated at concentrations of 100 μM, and incubated for 48 h and 72 h, respectively. Figure 3a and b indicate that without Sal A treatment, Aβ_{42} fibrils do not disaggregate. However, Fig. 3c and d show that Aβ_{42} fibrils are disaggregated by Sal A in dose-dependent manner. The 48 h pre-incubated Aβ_{42} fibrils are almost completely disaggregated after a further 24 h of incubation with 100 μM Sal A.

Sal A inhibits the aggregation of Aβ by stabilizing the α-helix structure at Aβ's C-terminus

Usually, Aβ's C-terminus tends to form a β-sheet in water, and the β-sheet causes Aβ aggregation [43]. The toxicity of Aβ depends on its capacity to form β-sheets [44]. The transformation process from α-helix to β-sheet at the Aβ C-terminus can be inhibited by small molecules [45,46]. CD experiments and MD simulations were conducted to elucidate the mechanism of Sal A-induced Aβ conformation transformation. The CD spectra were acquired for Aβ_{42}, with and without Sal A, at different incubation times (0 and 48 h) (Fig. 4). Freshly prepared Aβ_{42} in phosphate buffer solution (PBS) exhibits strong negative absorption around 200 nm, which indicates unfolded peptide structure; presumably, these proteins are in a monomeric state with random coil properties. After 48 h of incubation at 37°C, the Aβ_{42} CD spectrum reaches the maximal positive and negative absorptions, at 192 and 210 nm, respectively (Fig. 4). However, the

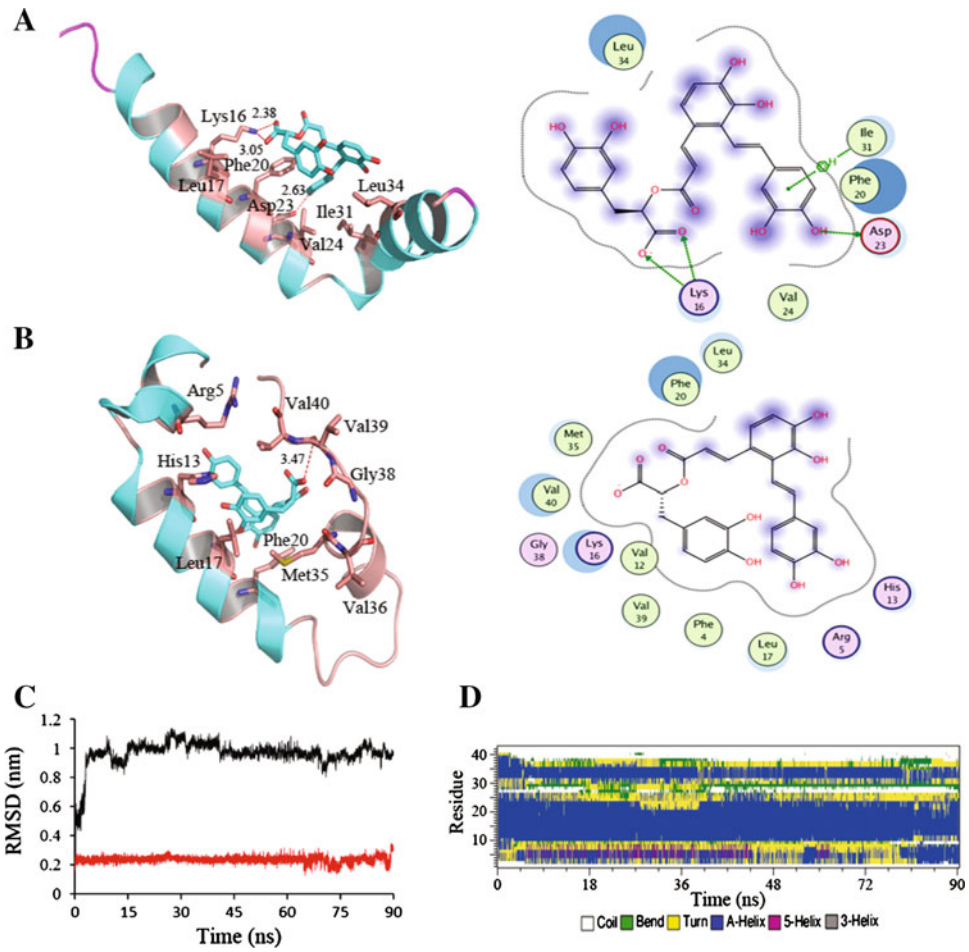

Fig. 5 Molecular dynamics (MD) simulations confirm that Sal A stabilizes the helix of Aβ. **a** The Sal A binding mode before MD simulations. **b** The Sal A binding mode after 90 ns MD simulations. A hydrogen bond is highlighted in *red dotted line*. **c** Aβ backbone atoms stabilization is confirmed by the RMSD curves. *Black curve* indicates that the backbone atoms in Aβ helix domain are stable after 15 ns simulations; *Red curve* indicates that Sal A conformation stays almost stationary **d** The time evolution of the secondary structures of Aβ_{42} in presence of Sal A

positive CD signals at 192 nm are attenuated after 50 μM Sal A has been added to the Aβ_{42} PBS solution.

The results of 90 ns MD simulations for the Aβ-Sal A complex demonstrate the details of Sal A's stabilization of Aβ secondary structure. Initially, Sal A binds to Aβ at its C-terminus, and forms three hydrogen bonds at residues Lys16 and Asp23 (Fig. 5a). After 90 ns MD simulations in water, Sal A is more deeply docked in the pocket of the helix and C-terminus. This complex of Sal A-Aβ is energetically more stable (Fig. 5b). The RMSD evolution curves (Fig. 5c) indicate that the complex became stabilized after 13 ns of simulation. The secondary conformation landscape of the complex demonstrates that the helix segment of Aβ conformation is dominant (56 %) (Fig. 5d colored in blue). This observation further proves that the helix of Aβ stays robust with Sal A in water. It is difficult to generate β-sheet conformation for Aβ when Sal A exists.

Sal A inhibits Aβ_{42} aggregation as a metal ion chelating agent

Metals have been shown to participate in the aggregation of Aβ peptides and enhance the formation of reactive oxygen species [17], thereby leading to neuronal death. Sal A UV spectra were acquired to determine if Sal A inhibits Aβ42 aggregation as a metal ion chelating agent. One of Sal A's UV characteristic peaks is located at 279 nm (Blue curve in Fig. 6a). When Sal A is mixed with Cu (II) or Fe (III), the peaks shift from 279 nm in different directions (green and purple curves in Fig. 6a). However, Zn (II) is unable to change the peak at 279 nm (Red curve in Fig. 6a). These observations confirm that Sal A chelates Fe (III) and Cu (II) ions.

Results from ThT experiments indicate that Cu (II), Fe (III), and Zn (II) ions can induce Aβ_{42} aggregation; this aggregation can be inhibited through Sal A chelation. However, Zn (II)-induced Aβ_{42} aggregation may occur through a different mechanism, as Sal A is not Zn (II)'s chelating agent.

Although Sal A chelated Cu and Fe ions, but not chelate Zn, it significantly decreases Cu, Fe or Zn ion-induced Aβ aggregation, thus suggesting that Sal A inhibits Aβ aggregation through and beyond its chelating metal action.

Sal A reduces the production of oxidative stress in SH-SY5Y cell lines

SH-SY5Y cells were incubated with Sal A in 100 μM, 50 μM, 25 μM, 12.5 μM, and 6.25 μM concentrations. The cells were also incubated with curcumin (the positive control), a known anti-oxidant, in the same concentration series. As shown in Fig. 7, the ROS is inhibited by Sal A in the dose-

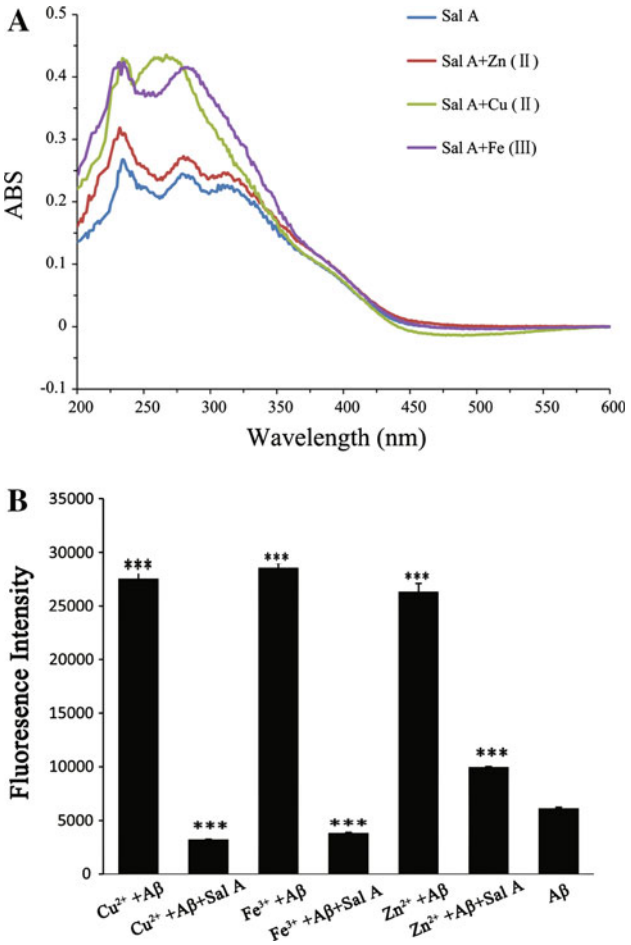

Fig. 6 Sal A inhibits metal-induced Aβ42 aggregation as metal ions chelating agent. **a** UV spectra of Sal A (1 mM), and Sal A with 1 mM Zn (II), or Cu (II), or Fe (III). **b** ThT fluorescence assays for determining Sal A inhibits Aβ_{42} aggregation induced by metal ions

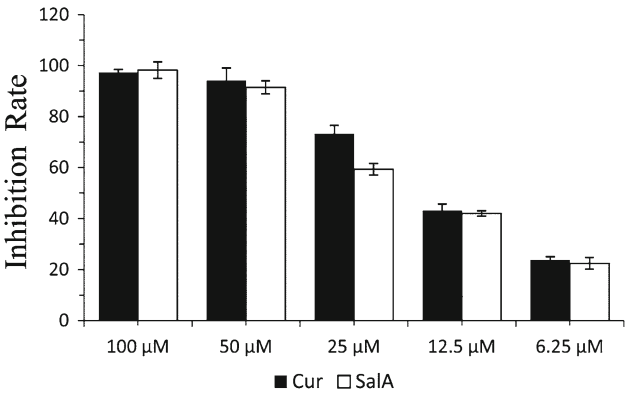

Fig. 7 Sal A inhibits ROS in SH-SY5Y cell lines in dose dependent manner. The results are represented in the percentage of control cells. The untreated cells were used as negative control, and curcumin was used as a positive control. Inhibition rate(%) = (1 − Fluorsencence Intensity of SalA/ Fluorsencence Intensity of control) × 100 %

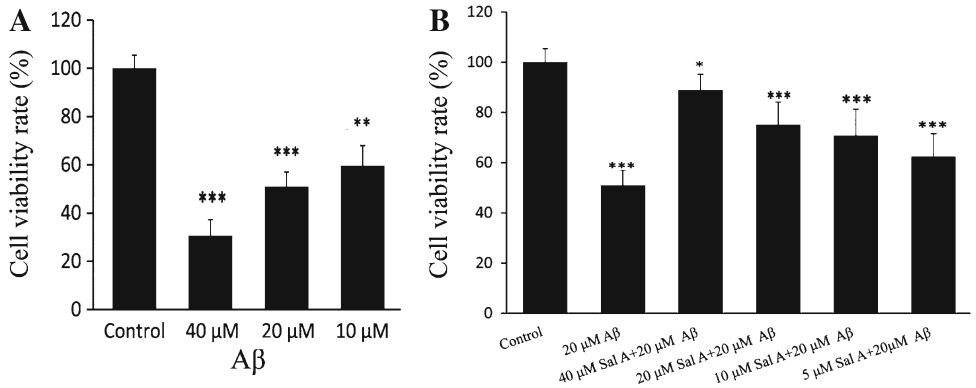

Fig. 8 Protective effect of Sal A on Aβ_{42}-induced toxicity in SH-SY5Y cell lines. **a** The pre-incubated Aβ_{42}(10, 20 and 40 μM) were added to the differentiated SH-SY5Y cells for 48 h. **b** The pre-incubated mixtures of Aβ_{42} (20 μM) with and without various concentrations of Sal A for 48 h. Cell viability was determined using MTT methods and data represented as mean ± SD of three independent experiments. Significant cytoprotective activity of Sal A was observed dose dependently at all tested concentrations (*$P < 0.05$, **$P < 0.01$)

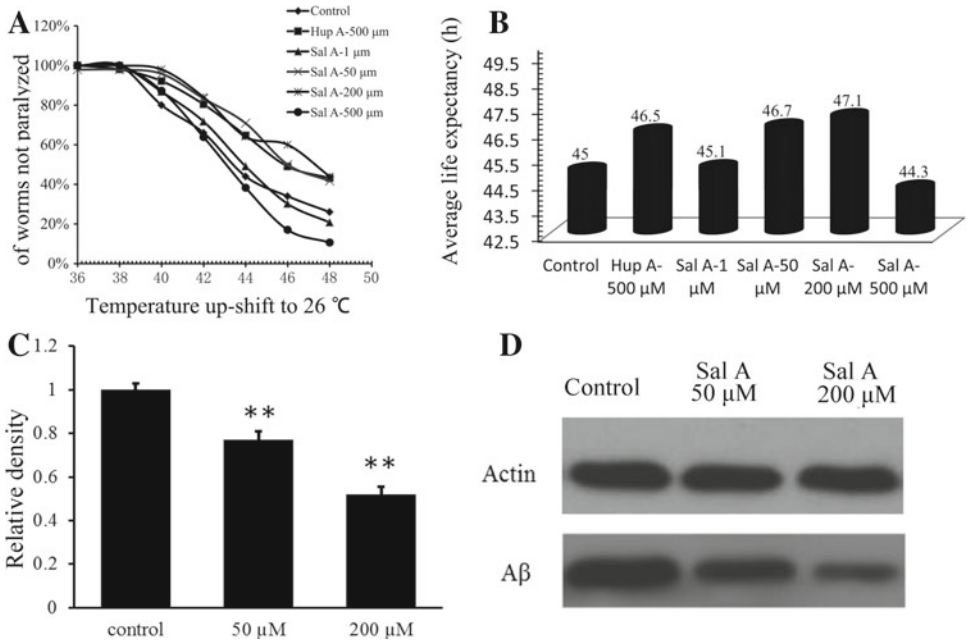

Fig. 9 Sal A eases Aβ-induced toxicity in muscle Aβ strain CL4176. **a** Time courses of paralysis assays in CL4176 fed with or without Sal A; **b** Average life span of CL4176 fed with or without Sal A. Synchronized eggs of CL4176 were maintained at 16 °C, on the 35 × 10 mm culture plates (~25eggs/plate) containing vehicle (Control), Huperzine A (Hup A, 500 μM), or Sal A (1, 50, 200 and 500 μM). **c** Quantification of immunoreactive total Aß in the CL4176 fed without or with Sal A (50 and 200 μM). Data are expressed relative density of an indicated band from three independent experiments. *Error bars* represent SEM. **$P < 0.05$. **d** Representative Western blot (BL) of total Aß in the CL4176 fed without or with Sal A (50 and 200 μM). The worms were collected, and immunoblotted with anti-Aß antibody (6E10). The hatched worms were grown for 48 h at 16°C followed by upshifting the temperature to 26°C to induce the transgene expression. The paralysis was scored at 2 h intervals. Data were measured in the percentage of non-paralyzed worms from at least three independent assays of 100 worms in each experiment

dependent manner, and the activities of Sal A and curcumin are almost the same.

Sal A protects cells against Aβ_{42}-induced toxicity

SH-SY5Y cells were treated with Aβ_{42} solutions in 10 μM, 20 μM, and 40 μM concentrations. Figure 8a demonstrates that Aβ significantly reduces the cell viability (Aβ-induced cytotoxicity) in dose-dependent manner. Figure 8b exhibits that the cells are well protected when 20 μM Aβ is mixed with Sal A in 5 μM, 10 μM, 20 μM, and 40 μM concentrations. This concludes that Sal A is a neuroprotective agent against Aβ_{42}-induced toxicity in a dose-dependent manner.

Sal A reduces total Aβ and alleviates Aβ-induced paralysis in transgenic *C. elegans* strain CL4176

Transgenic *C. elegans* were fed with Sal A to determine if Sal A can ease Aβ-induced toxicity *in vivo*. Figure 9a and b demonstrate that Sal A significantly delays Aβ-induced paralysis at dosages of 50 and 200 μM. Huperzine A (Hup A), an acetylcholinesterase (AChE) inhibitor, was also tested as a positive control. The activity of 50 μM Sal A is equivalent to 500 μM Hup A's.

To determine whether Sal A treatment affected the total Aβ levels in the worm, we measured levels of Aβ using antibody 6E10. Figure 9c and d shows that Sal A, at 50 and 200 μM concentrations, significantly decreases the total Aβ ($p = 0.005$ and 0.008 μM respectively). This study is thus the first to disclose that Sal A attenuates Aβ-induced paralysis in *C. elegans* strain CL4176 through decreasing the levels of total Aβ.

Conclusions

In this paper, for the first time, we report that Sal A significantly inhibits the formation of Aβ fibrils. Moreover, Sal A dose dependently destabilizes aggregated Aβ fibrils in vitro, which is proved by ThT dying and TEM imaging studies. Sal A inhibits Aβ aggregation by blocking the conversion of the α-helices into β-sheets, as shown from CD spectrum and MD simulations. Although Sal A chelated Cu and Fe ions, but not chelate Zn, it significantly decreases Cu, Fe or Zn ion-induced Aβ aggregation, thus suggesting that Sal A inhibits Aβ aggregation through and beyond its chelating metal action. Sal A also demonstrates antioxidative activity and neuroprotective activity in SH-SY5Y cells. Sal A alleviates Aβ-induced paralysis in *C. elegans* strain CL4176. Together with our findings from ThT, CD, and EM analysis, our results suggest that Sal A ameliorates Aβ toxicity in transgenic *C. elegans* strain CL4176 by reducing amounts of the toxic form of Aβ. To sum up, because of its multiple mechanisms of action, Sal A is a promising multifunctional agent for the treatment of AD.

Acknowledgments This work was funded in part of the National Natural Science Foundation of China (No. 81001372, 81173470), the National High-tech R&D Program of China (863 Program) (2012AA020307), the introduction of innovative R&D team program of Guangdong Province (No. 2009010058), and the External Cooperation Program of Chinese Academy of Sciences (No. P2010-KF08). Some strains were provided by the CGC, which was funded by NIG Office of Research Infrastructure Programs (P40 OD010440). The authors thank Dr. Chaolun Liang for the assistance with TEM assay.

Conflict of interest The authors declare no competing financial interest.

References

1. Selkoe DJ (2000) The genetics and molecular pathology of Alzheimer's disease–roles of amyloid and the presenilins. Neurol Clin 18:903–922. doi:10.1016/S0733-8619(05)70232-70232
2. Carter J, Anderton B (1994) Molecular pathology of Alzheimer's disease. Brit J Hosp Med 51:522–528
3. Selkoe DJ (2004) Cell biology of protein misfolding: the examples of Alzheimer's and Parkinson's diseases. Nat Cell Biol 6: 1054–1061. doi:10.1038/Ncb1104-1054
4. Okonkwo AI, Li B, Takezaki M, Arbiser JL, Pace BS (2013) Discovery of novel fetal hemoglobin inducing drugs to treat sickle cell disease. J Invest Med 61:464–465
5. Finder VH (2010) Alzheimer's disease: a general introduction and Pathomechanism. J Alzheimers Dis 22:S5–S19. doi:10.3233/Jad-2010-100975
6. McGeer PL, McGeer EG (1999) Inflammation of the brain in Alzheimer's disease: implications for therapy. J Leukocyte Biol 65:409–415
7. Galasko D, Montine TJ (2010) Biomarkers of oxidative damage and inflammation in Alzheimer's disease. Biomark Med 4:27–36. doi:10.2217/Bmm.09.89
8. Religa D, Strozyk D, Cherny RA, Volitakis I, Haroutunian V, Winblad B, Naslund J, Bush AI (2006) Elevated cortical zinc in Alzheimer disease. Neurology 67:69–75. doi:10.1212/01.wnl.0000223644.08653.b5
9. Pierre JL, Fontecave M (1999) Iron and activated oxygen species in biology: the basic chemistry. Biometals 12:195–199. doi:10.1023/A:1009252919854
10. Bush AI, Tanzi RE (2008) Therapeutics for Alzheimer's disease based on the metal hypothesis. Neurotherapeutics 5:421–432. doi:10.1016/j.nurt.2008.05.001
11. Jakob-Roetne R, Jacobsen H (2009) Alzheimer's disease: from pathology to therapeutic approaches. Angew Chem Int Ed 48:3030–3059. doi:10.1002/anie.200802808
12. Scott LE, Orvig C (2009) Medicinal inorganic chemistry approaches to passivation and removal of aberrant metal ions in disease. Chem Rev 109:4885–4910. doi:10.1021/Cr9000176
13. Smith MA, Harris PL, Sayre LM, Perry G (1997) Iron accumulation in Alzheimer disease is a source of redox-generated free radicals. Proc Natl Acad Sci USA 94:9866–9868. doi:10.1073/pnas.94.18.9866
14. Perry G, Taddeo MA, Petersen RB, Castellani RJ, Harris PLR, Siedlak SL, Cash AD, Liu Q, Nunomura A, Atwood CS, Smith MA (2003) Adventiously-bound redox active iron and copper are at the center of oxidative damage in Alzheimer disease. Biometals 16:77–81. doi:10.1023/A:1020731021276
15. Choi JS, Braymer JJ, Nanga RPR, Ramamoorthy A, Lim MH (2010) Design of small molecules that target metal–a beta species and regulate metal-induced A beta aggregation and neurotoxicity. Proc Natl Acad Sci USA 107:21990–21995. doi:10.1073/pnas.1006091107
16. Lannfelt L, Blennow K, Zetterberg H, Batsman S, Ames D, Hrrison J, Masters CL, Targum S, Bush AI, Murdoch R, Wilson J, Ritchie CW, Grp PES (2008) Safety, efficacy, and biomarker findings of PBT2 in targeting A beta as a modifying therapy for Alzheimer's disease: a phase IIa, double-blind, randomised, placebo-controlled trial. Lancet Neurol 7:779–786. doi:10.1016/S1474-4422(08)70167-4
17. Ritchie CW, Bush AI, Mackinnon A, Macfarlane S, Mastwyk M, MacGregor L, Kiers L, Cherny R, Li QX, Tammer A, Carrington D, Mavros C, Volitakis I, Xilinas M, Ames D, Davis S, Volitakis I, Xilinas M, Ames D, Davis S, Beyreuther K, Tanzi RE, Masters CL (2003) Metal-protein attenuation with iodochlorhydroxyquin (clioquinol) targeting A beta amyloid deposition and toxic-

ity in Alzheimer disease–a pilot phase 2 clinical trial. Arch Neurol 60:1685–1691. doi:10.1001/archneur.60.12.1685
18. Arbiser JLKS, van Leeuwen R, Hurwitz SJ, Selig M, Dickersin GR, Flint A, Byers HR, Chen LB (1998) Clioquinol-zinc chelate: a candidate causative agent of subacute myelo-optic neuropathy. Mol Med 4:665–670
19. Praticò D, Delanty N (2000) Oxidative injury in diseases of the central nervous system: focus on alzheimer's disease. Am J Med 109:577–585. doi:10.1016/S0002-9343(00)00547-7
20. Allan Butterfield D (2002) Amyloid β-peptide (1–42)-induced oxidative stress and neurotoxicity: implications for neurodegeneration in Alzheimer's disease brain. A review. Free Radic Res 36:1307–1313. doi:10.1080/1071576021000049890
21. Castegna A, Thongboonkerd V, Klein JB, Lynn B, Markesbery WR, Butterfield DA (2003) Proteomic identification of nitrated proteins in Alzheimer's disease brain. J Neurochem 85:1394–1401. doi:10.1046/j.1471-4159.2003.01786.x
22. Chong ZZ, Li FQ, Maiese K (2005) Oxidative stress in the brain: Novel cellular targets that govern survival during neurodegenerative disease. Prog Neurobiol 75:207–246. doi:10.1016/j.pneurobio.2005.02.004
23. Petersen RB, Nunomura A, Lee H, Casadesus G, Perry G, Smith MA, Zhu XW (2007) Signal transduction cascades associated with oxidative stress in Alzheimer's disease. J Alzheimers Dis 11:143–152
24. Praticò D (2008) Oxidative stress hypothesis in Alzheimer's disease: a reappraisal. Trends Pharmacol Sci 29:609–615. doi:10.1016/j.tips.2008.09.001
25. Ono K, Hasegawa K, Naiki H, Yamada M (2006) Anti-Parkinsonian agents have anti-amyloidogenic activity for Alzheimer's beta-amyloid fibrils in vitro. Neurochem Int 48:275–285. doi:10.1016/j.neuint.2005.11.001
26. Kim DD, Lee CY (2004) Comprehensive study on vitamin C equivalent antioxidant capacity (VCEAC) of various polyphenolics in scavenging a free radical and its structural relationship. Crit Rev Food Sci 44:253–273. doi:10.1080/10408690490464960
27. Markesbery WR (1997) Oxidative stress hypothesis in Alzheimer's disease. Free Radical Bio Med 23:134–147. doi:http://dx.doi.org/10.1016/S0891-5849(96)00629-6
28. Liu CL, Xie LX, Li M, Durairajan SS, Goto S, Huang JD (2007) Salvianolic acid B inhibits hydrogen peroxide-induced endothelial cell apoptosis through regulating PI3K/Akt signaling. PloS one 2:e1321. doi:10.1371/journal.pone.0001321
29. Du GH, Zhang JT (1995) Protective effects of salvianolic acid A against impairment of memory induced by cerebral ischemia-reperfusion in mice. Yao xue xue bao 30:184–190. doi:10.3321/j.issn:0513-4870.1995.10.001
30. Wang XJ, Xu JX (2005) Salvianic acid A protects human neuroblastoma SH-SY5Y cells against MPP+-induced cytotoxicity. Neurosci Res 51:129–138. doi:10.1016/j.neures.2004.10.001
31. Oh KS, Oh BK, Mun J, Seo HW, Lee BH (2011) Salvianolic acid A suppress lipopolysaccharide-induced NF-kappaB signaling pathway by targeting IKKbeta. Int Immunopharmacol 11:1901–1906. doi:10.1016/j.intimp.2011.07.022
32. Sperl B, Seifert MH, Berg T (2009) Natural product inhibitors of protein-protein interactions mediated by Src-family SH2 domains. Bioorg Med Chem Lett 19:3305–3309. doi:10.1016/j.bmcl.2009.04.083
33. Zhang HA, Gao M, Zhang L, Zhao Y, Shi LL, Chen BN, Wang YH, Wang SB, Du GH (2012) Salvianolic acid A protects human SH-SY5Y neuroblastoma cells against H_2O_2-induced injury by increasing stress tolerance ability. Biochem Bioph Res Co 421:479–483. doi:10.1016/j.bbrc.2012.04.021
34. Coles M, Bicknell W, Watson AA, Fairlie DP, Craik DJ(1998) Solution structure of amyloid beta-peptide(1–40) in a water-micelle environment. Is the membrane-spanning domain where we think it is? Biochemistry 37:11064–11077. doi:10.1021/bi972979f
35. Molecular modeling software. SYBYL 7.3, Tripos, St. Louis, MO. (2006)
36. Cheng A, Best SA, Merz KM, Reynolds CH (2000) GB/SA water model for the Merck molecular force field (MMFF). J Mol Graph Model 18:273–282. doi:10.1016/S1093-3263(00)00038-3
37. Accelrys Discovery Studio 2.5. Accelrys Int, San Diego, CA. (2009)
38. Crump JA, Scott LE, Msuya E, Morrissey AB, Kimaro EE, Shao JF, Stevens WS (2009) Evaluation of the Abbott m2000rt Real-Time (TM) HIV-1 assay with manual sample preparation compared with the ROCHE COBAS (R) AmpliPrep (TM)/AMPLICOR (TM) HIV-1 MONITOR (R) v1.5 using specimens from East Africa. J Virol Methods 162:218–222. doi:10.1016/j.jviromet.2009.08.013
39. Abraham MJ, Gready JE (2011) Optimization of parameters for molecular dynamics Simulation using smooth particle-Mesh Ewald in GROMACS 4.5. J Comput Chem 32:2031–2040. doi:10.1002/Jcc.21773
40. Duan Y, Wu C, Chowdhury S, Lee MC, Xiong GM, Zhang W, Yang R, Cieplak P, Luo R, Lee T, Caldwell J, Wang JM, Kollman P (2003) A point-charge force field for molecular mechanics simulations of proteins based on condensed-phase quantum mechanical calculations. J Comput Chem 24:1999–2012. doi:10.1002/jcc.10349
41. Zhang YH, Wooster MJ, Tutubalina O, Perry GLW (2003) Monthly burned area and forest fire carbon emission estimates for the Russian Federation from SPOT VGT. Remote Sens Environ 87:1–15. doi:10.1016/S0034-4257(03)00141-X
42. Gaussian03, Revision C.02. Gaussian, Inc., Wallingford CT (2004).
43. Yang F, He K, Liu K (2009) Removal of the colloidal impurities in the purification of salvianolic acid B. Chin J Chromatogr 27:379–381
44. Lorenzo A, Yankner BA (1994) Beta-amyloid neurotoxicity requires fibril formation and is inhibited by congo red. Proc Natl Acad Sci USA 91:12243–12247. doi:10.1073/pnas.91.25.12243
45. Yang C, Zhu XL, Li JY, Shi RW (2010) Exploration of the mechanism for LPFFD inhibiting the formation of beta-sheet conformation of A beta(1–42) in water. J Mol Model 16:813–821. doi:10.1007/s00894-009-0594-y
46. Wang B, Liu JX, Meng HX, Lin CR (2012) Blocking effect of salvianolic acid A on calcium channels in isolated rat ventricular myocytes. Chin J Integr Med 18:366–370. doi:10.1007/s11655-011-0707-1